Chemical Engineering and Processing 65 (2013) 45–52

Contents lists available at SciVerse ScienceDirect

Chemical Engineering and Processing: Process Intensification

journal homepage: www.elsevier.com/locate/cep

Characterization of a bipolar parallel-plate electrochemical reactor for water disinfection using low conductivity drinking water

E.R. Henquín[a], A.N. Colli[a], M.E.H. Bergmann[b], J.M. Bisang[a,*]

[a] Universidad Nacional del Litoral, Santiago del Estero 2829, S3000AOM Santa Fe, Argentina
[b] Anhalt University, Bernburger Straße 55, D-06366 Köthen/Anhalt, Germany

ARTICLE INFO

Article history:
Received 10 August 2012
Received in revised form 3 December 2012
Accepted 26 December 2012
Available online 18 January 2013

Keywords:
Bipolar electrodes
Drinking water disinfection
Electrochemical reactors
Parallel plate electrodes

ABSTRACT

A reactor was built, experimentally studied and modelled having six bipolar electrodes placed between the terminal ones, all of them were RuO_2/IrO_2 on a Ti sheet. The interelectrode gap was 1.5 mm. Plastic plates were optionally arranged in the inlet and outlet to the electrodes to produce entrance or exit regions. The Laplace equation was numerically solved for the solution phase to obtain the current and potential distribution. The calculations performed without entrance and exit regions show that the current distribution is pronounced at the thickness of the electrodes and at the electrode edges. The presence of the entrance and exit regions covers the electrode thickness, increases the current distribution and diminishes the leakage current. The hydrodynamics of the reactor was analyzed by the stimulus–response method and the best behaviour was obtained when the equipment was filled with glass beads. This reactor was tested analyzing the in-line production of sodium hypochlorite from drinking water. In a typical galvanostatic experiment, carried out at 10.3 A, with a volumetric flow rate of 2 $dm^3\ min^{-1}$ the hypochlorite concentration at the exit was 25 $mg\ dm^{-3}$. In this case, the applied potential difference was 128 V and the current efficiency was 4.3%.

1. Introduction

Electrochemical disinfection of water has received considerable attention in the literature. Recently, Bergmann [1] and Bergmann et al. [2] summarized the state of the art related to fundamental studies and the formation of products and inorganic by-products. Thus, the promising results of this technology claim for an efficient design and optimization of the electrochemical reactors, which must work under unusual operating conditions, i.e. the desired reactions are of lower extent than the parasitic ones, low conductivity of the electrolyte, and frequently it is required a reactor of small size in comparison with traditional electrochemical processes. Kraft [3], in a short review, described several commercial electrochemical disinfection devices for different applications. In general, it must be distinguished between arrangements for disinfecting water in a flow-through regime and for killing of microorganisms naturally or artificially adhered to surfaces (treatment of biofilms by polarization of the surface). For example, a cylindrical reactor, made by winding concentrically two sheets of carbon cloth separated by two ion-exchange membranes, was used to test the sterilization of drinking water [4], where the electrochemical disinfection was attributed to the direct oxidation of intracellular coenzyme A and not to the electrochemical generation of disinfectants. This method was also used in a system employing activated carbon fibres [5] as electrodes in a cylindrical reactor and titanium nitride meshes [6] as three-dimensional anodes and cathodes placed alternatively in a titanium pipe.

A disinfecting process, without the mediation of active chlorine, was analyzed using boron-doped diamond anodes in a stirred tank electrochemical reactor [7], whose mass-transfer performance and hydrodynamic behaviour were reported. The effectiveness of the process was attributed to the simultaneous formation of ozone and hydrogen peroxide as strong oxidizing agents.

The configuration with parallel-plate electrodes was also considered as an appropriate geometry for electrochemical water disinfection. Thus, the Zappi™ electrochemical cell [8], consisting of two platinum clad niobium mesh anodes and two steel cathodes in an open configuration, was used to evaluate the efficacy of an electrochemical disinfection technology. Likewise, the performance of the commercial filter-press reactor, EC Electro MP-Cell, in a single compartment with two electrodes was analyzed using as anode either a boron-doped diamond electrode or a DSA and stainless steel as cathode [9]. Furthermore, the hydrodynamic behaviour complemented with mass-transfer studies was reported in [10], where the reactor was tested according to a single pass configuration and also as a recirculating electrochemical system. For a wide range of experimental conditions a good agreement between model prediction and experimental data was achieved,

* Corresponding author. Tel.: +54 342 4571164; fax: +54 342 4571164.
E-mail address: jbisang@fiq.unl.edu.ar (J.M. Bisang).

0255-2701/$ – see front matter © 2013 Elsevier B.V. All rights reserved.
http://dx.doi.org/10.1016/j.cep.2012.12.007

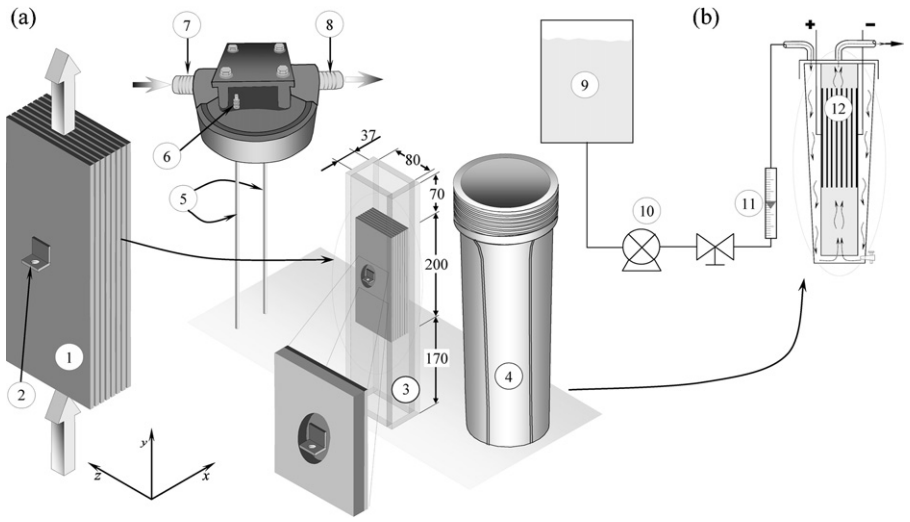

Fig. 1. (a) Exploded view of the electrochemical reactor: (1) electrode stack; (2) electrical connection to the terminal electrodes; (3) holder for the electrode stack; (4) container for holding water; (5) current feeders; (6) external electrical connection; (7) water inlet; (8) water outlet. (b) Scheme of the hydraulic system: (9) water reservoir; (10) centrifugal pump; (11) flowmeter; (12) electrochemical reactor. Dimensions in mm.

when a non-ideal flow behaviour was assumed as a combination of ideal flow reactors, bypass flow elements, and dead zones. The bacterial inactivation in the absence of chlorine compounds using a thin layer electrochemical cell with a dimensionally stable anode (70% TiO_2–30% RuO_2) and a stainless steel 304 cathode was studied in [11] without the generation of chlorine. The procedure is efficient but requires the combination with other methods to fulfil the legal regulations.

Recently [12], a multiwalled carbon nanotube microfilter was successfully tested as anode in an electrochemical cell for both pathogen removal and inactivation. Patent literature still offers a large variety of different reactor configurations. Unfortunately, no information on application exists on these variants. The hypochlorite electro-generation was extensively analyzed in the open and patent literature, reviewed by Ibl and Vogt [13], to use this strong oxidizing agent for a range of applications.

In the reactors described above, the electrodes are frequently connected in a monopolar arrangement, where they have a single polarity, either anodes or cathodes. Kodym et al. [14,15] considered the effect of geometrical factors on the current distribution in electrolysis cells for direct drinking water disinfection. In spite of the good performance of the monopolar devices, an external electrical connection at each electrode of the reactor is required, which can be troublesome. In order to circumvent this difficulty, a bipolar connection is attractive. Electrochemical reactors with bipolar parallel plate electrodes are profusely used in the industrial practice and the state of the art is properly shown by Pletcher and Walsh [16]. However, the bipolar configuration shows as drawback the leakage current, which can bypasses the electrodes flowing through the solution phase outside the interelectrode gap without to produce electrochemical reactions at the bipolar electrodes. Then, an appropriate design of the electrochemical reactor is required to minimize this negative aspect.

The aim of the present paper is to apply experimental and modelling methods with respect to a bipolar electrochemical reactor equipped with parallel-plate electrodes for drinking water disinfection to assess and optimize its performance. Thus, the use of procedures to determine the current and residence time distributions allows a rational optimization of the equipment and then its disinfection capability is tested taking into account the in-line production of hypochlorite.

2. Experimental

Fig. 1 schematically shows the drinking water disinfection reactor (supplier Dr. Rittel Verfahrenstechnik GmbH, Grossbadegast) formed by six bipolar electrodes placed between the terminal electrodes. All the electrodes were RuO_2/IrO_2 on Ti (Heraeus) and had the same dimensions, 80 mm wide, 200 mm long and 3.25 mm thick. The active layer of 2 μm thickness is characterized by a molar ratio Ru:Ir of 75%:25%. The electrodes were inserted in a PVC plastic holder to obtain mechanical stability of the pack and to fix the interelectrode space, 1.5 mm. The geometric surface area at each electrode side was 159 cm^2. The electrode stack was placed inside a water filter housing, made from reinforced polypropylene, and the water flow was upwards. PVC plastic plates can be arranged in the inlet and outlet to the electrodes in order to produce more defined entrance or exit regions. The dimensions of the plastic plates were 80 mm wide, 165 mm long at the entrance and 65 mm long at the exit. The reactor was made part of a flow circuit system, sketched in Fig. 1(b), consisting of a reservoir, a pump, a flow meter, and a valve to control the water flow rate. This reactor was tested analyzing the in-line production of sodium hypochlorite from regional drinking water (Köthen/Anhalt), which composition is summarized in Table 1. The experiments were done under galvanostatic control. Samples of water were taken at the reactor outlet and the hypochlorite concentration was spectrophotometrically determined using an Analytic Jena, Specord 40, UV Spectrophotometer with a 50 mm quartz absorption cell. The measurements were made at a wavelength of 290 nm and the hypochlorite concentration was calculated using the Lambert–Beer law with a molar absorption

Table 1
Composition of drinking water.

Chloride (mg dm^{-3})	40
Sulphate (mg dm^{-3})	145–165
Nitrate (mg dm^{-3})	10–13.9
Calcium (mg dm^{-3})	104
Magnesium (mg dm^{-3})	21
Potassium (mg dm^{-3})	2
Sodium (mg dm^{-3})	19
TOC (mg dm^{-3})	1.8
pH	7.4–7.9

coefficient of $(350 \pm 15)\,dm^3\,mol^{-1}\,cm^{-1}$ [17]. The experiments were performed at volumetric flow rates ranging from 1.78 to 7.21 $dm^3\,min^{-1}$, which represents mean electrolyte velocities in the interelectrode gap from 0.035 to 0.143 $m\,s^{-1}$ and Reynolds numbers, calculated with the hydraulic diameter, in the range 104–421.

The residence time distribution was analyzed using the stimulus-response method. As a stimulus, an impulse function was simulated by manually injecting a saturated KCl solution, 1 cm^3, into the inlet for a short time [18]. The electrolytic conductivity was monitored by means of a flow conductivity cell, WTW model TetraCon 96. The conductometer was connected to a digital multimeter to obtain conductance versus time. It was verified that a linear relation between conductivity and concentration takes place in the measure range.

3. Results and discussion

3.1. Primary current distribution studies

The potential difference applied at each reactor of the stack comprises the reversible cell voltage, the overpotentials at both electrodes and the ohmic drop in the solution phase. Due to the high value of resistivity of drinking water, approximately 2000 Ω cm, the bipolar Wagner number for the present reactor is very small, ranging from 1×10^{-7} to 1×10^{-5}. After that, according to [19] for bipolar Wagner numbers lower than 1×10^{-3}, it is expected that the secondary current distribution is close to the primary one. Moreover, the potential difference at each interface between electrode and solution was disregarded because, at the high currents interesting for technical operation, the ohmic drop in the solution phase is the dominant term in the potential balance, which justifies considering the system as a resistive one. Then, the kinetic and thermodynamic properties of the electrochemical reactions were ignored. Although, in this study primary current distributions are reported, which represents the simplest mathematical treatment, the essential features of current distribution are maintained and the reactor can be properly represented under the usual operating conditions.

The potential distribution was obtained by solving the Laplace equation in the solution phase including the electrolyte outside the interelectrode gap:

$$\frac{\partial^2\phi(x,y)}{\partial x^2} + \frac{\partial^2\phi(x,y)}{\partial y^2} = 0 \tag{1}$$

where ϕ (V) is the potential in the solution phase and x (m) and y (m) are the axial coordinates. The current distribution in the direction of the electrode width, z coordinate in Fig. 1(a), is neglected for symmetry. Eq. (1) was numerically solved by using the finite difference method with an equidistant grid and taking into account the following boundary conditions:

$$\phi = U_A \tag{2}$$

$$\phi = U_C \tag{3}$$

being U_A and U_C the potentials in the solution phase adjacent to the terminal anode and cathode, respectively.

At the insulating walls is:

$$\left.\frac{\partial\phi}{\partial p}\right|_{\text{insulating walls}} = 0 \tag{4}$$

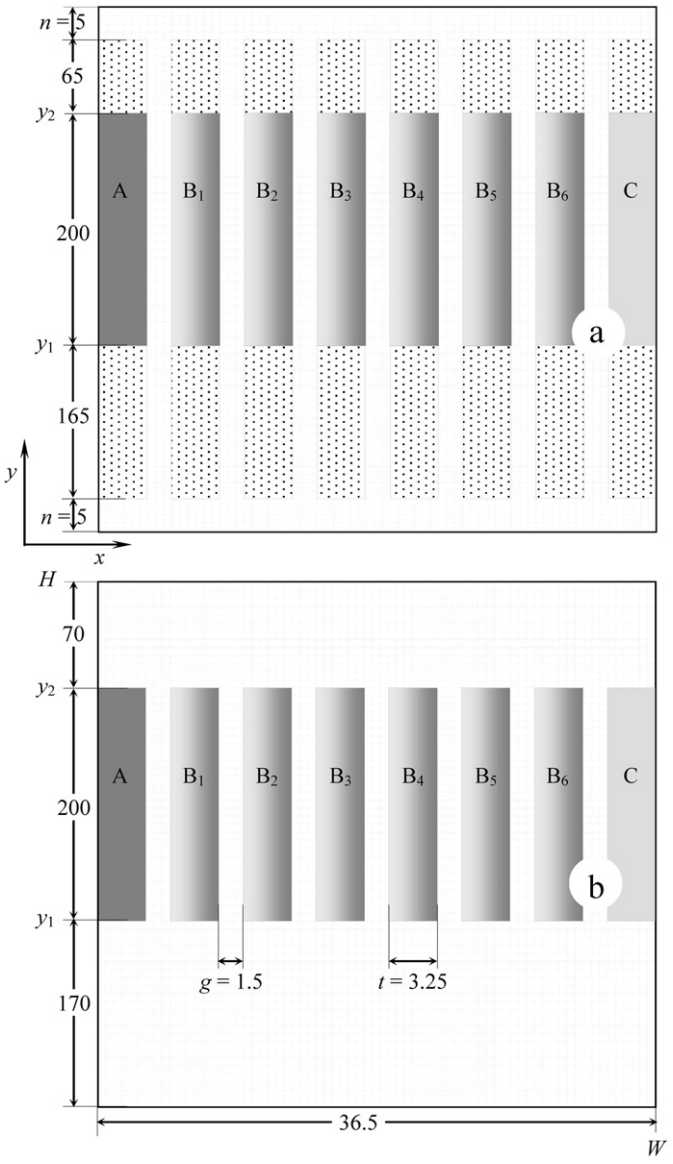

Fig. 2. Schematic representation of the stack of electrodes. (a) With entrance and exit regions. Shading rectangles: electrodes. Dotted rectangles: plastic plates for the entrance and exit regions. (b) Without entrance and exit regions. g, interelectrode gap; H, reactor height; n, space for the flow distribution; t, electrode thickness; W, reactor width in the direction of current flow. Dimensions in mm.

p being the perpendicular coordinate to the wall. Likewise, at the electrode surfaces the local current density, j ($A\,m^{-2}$), can be calculated as

$$j_{i,k} = -\frac{1}{\rho}\left.\frac{\partial\phi}{\partial p}\right|_{k\text{th electrode surface}} \tag{5}$$

here i indicates the anodic or the cathodic electrode side, k the electrode, i.e. terminal anode (A), bipolar electrodes (B_j) or terminal cathode (C), and ρ (Ω m) is the electrolyte resistivity. The effect of the gases generated at the electrodes on the electrolyte resistivity is disregarded.

The current drained at each electrode surface was calculated as

$$I_k = \int_S j_{i,k}\,dS \tag{6}$$

where S (m^2) is the electrode surface area of a given polarity.

To evaluate the local current density the four potential points in the solution phase nearest to each electrode surface were fitted with the polynomial [20]:

$$\phi = a_0 + a_1 p + a_2 p^2 + a_3 p^3 \tag{7}$$

where p is measured from the electrode surface. Introducing the first derivative of Eq. (7), evaluated at the electrode surface, in Eq. (5) the local current density at a given electrode surface is given by:

$$j = -\frac{a_1}{\rho} \tag{8}$$

Thus, the current density distribution results in

$$\frac{j(l)}{j_{\text{mean}}} = \frac{a_1(l)}{W/S \int_{S/W} a_1(l)\mathrm{d}l} \tag{9}$$

where W is the electrode width and l (m) represents a coordinate along the electrode surface, i.e. l agrees with y for the vertical region of a electrode and with x for the horizontal ones.

The solution of the above equations was performed with a home-made software [21] utilizing the scientific computing platform Matlab. Two configurations, sketched in Fig. 2, were studied. In the first, shown in Fig. 2(a) and called system with entrance and exit regions, plastic plates are arranged at the inlet and outlet to the electrodes. In the second one, Fig. 2(b) and called system without entrance and exit regions, the plastic plates were removed and the space filled with electrolyte.

The effect of the entrance and exit regions on the potential distribution for both arrangements is shown in Fig. 3, where it can be seen six zones with a constant potential value corresponding to the metal phase of each bipolar electrode, and an approximately linear variation is detected in the interelectrode gap. Likewise, Fig. 3(a) shows that in the configuration with entrance and exit regions the leakage current produces a linear variation of potential in the solution phase between the plastic plates and the insets report the potential variation in the lower and upper parts of the reactor, including the spaces for the flow distribution, where the potential distribution is in accordance with Eq. (4). For the configuration without plastic plates at the entrance and exit regions, Fig. 3(b) reports a pronounce potential variation in the solution phase near the edges of the electrodes and outside the interelectrode gap, which approaches a constant value in the neighbourhood of the top and bottom of the reactor.

Fig. 4 reports the current distribution for both configurations. It is observed that the current distribution is pronounced at the electrode edges, which represents only the 0.5% of the electrode length. Then, the major part of the electrode surface shows a constant current density. When the plastic plates are removed, the current distributions are extremely marked at the thickness of the electrodes, as it is reported by the side plots in Fig. 4(b). Furthermore, Fig. 5 compares the current distribution at the lower electrode edge for all the electrodes at both configurations, where $B_{a,j}$ denotes the anodic side of the jth bipolar electrode and $B_{c,j}$ its cathodic side. For symmetry, both terminal electrodes show identical current distributions. The same behaviour is detected between the cathodic side of the first bipolar electrode and the anodic side of the last bipolar electrode and also for all the bipolar surfaces with contrary polarity and symmetrically positioned. Fig. 5 reports that the current distribution for the configuration with entrance region is more pronounced than that without the plastic plates, because in this last case a fraction of the current is drained at the electrode thickness. A similar behaviour was reported for the presence of insulating edge strips along the side of the electrodes in zinc electrowinning cells [22], where the removal of the edge strip evens out the current distribution remarkably.

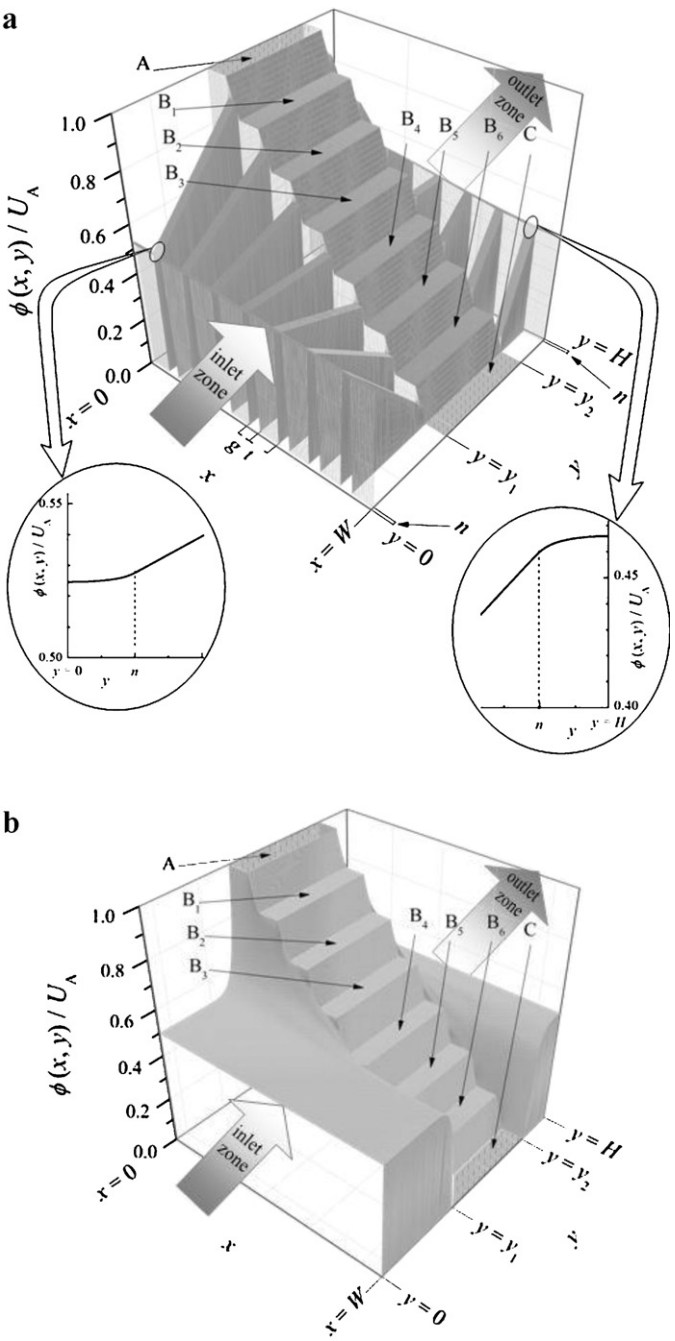

Fig. 3. Potential distribution for the water disinfection reactor: (a) with entrance and exit regions; (b) without entrance and exit regions. References according to Fig. 2.

Fig. 6 compares the current at each electrode for both configurations. The bipolar electrodes in the electrochemical system without the plastic plates drain only about the 98% of the cell current. However, when plastic plates are arranged at the inlet and outlet of the electrodes the leak of current at each electrode diminishes to 0.1%. Thus, the entrance and exit regions become more efficient the reactor and allow to fulfil the criterion related to the permissible amount of leakage current in bipolar electrochemical reactors according to Bergner and Hannesen [23]. However, as can be seen in Section 3.3 most part of current is consumed in side reactions being different from chlorine species formation. So, negligible influence of entrance or exit region conditions should be expected on disinfectant production.

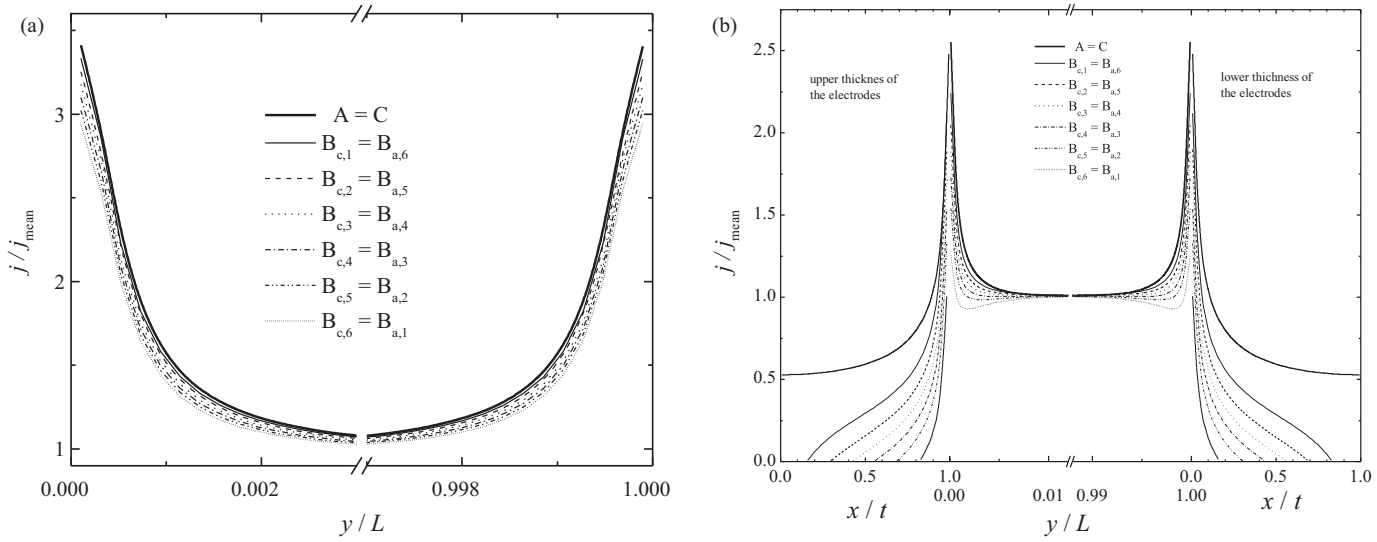

Fig. 4. Current density distribution at the electrode surfaces: (a) with entrance and exit regions; (b) without entrance and exit regions. References according to Fig. 2.

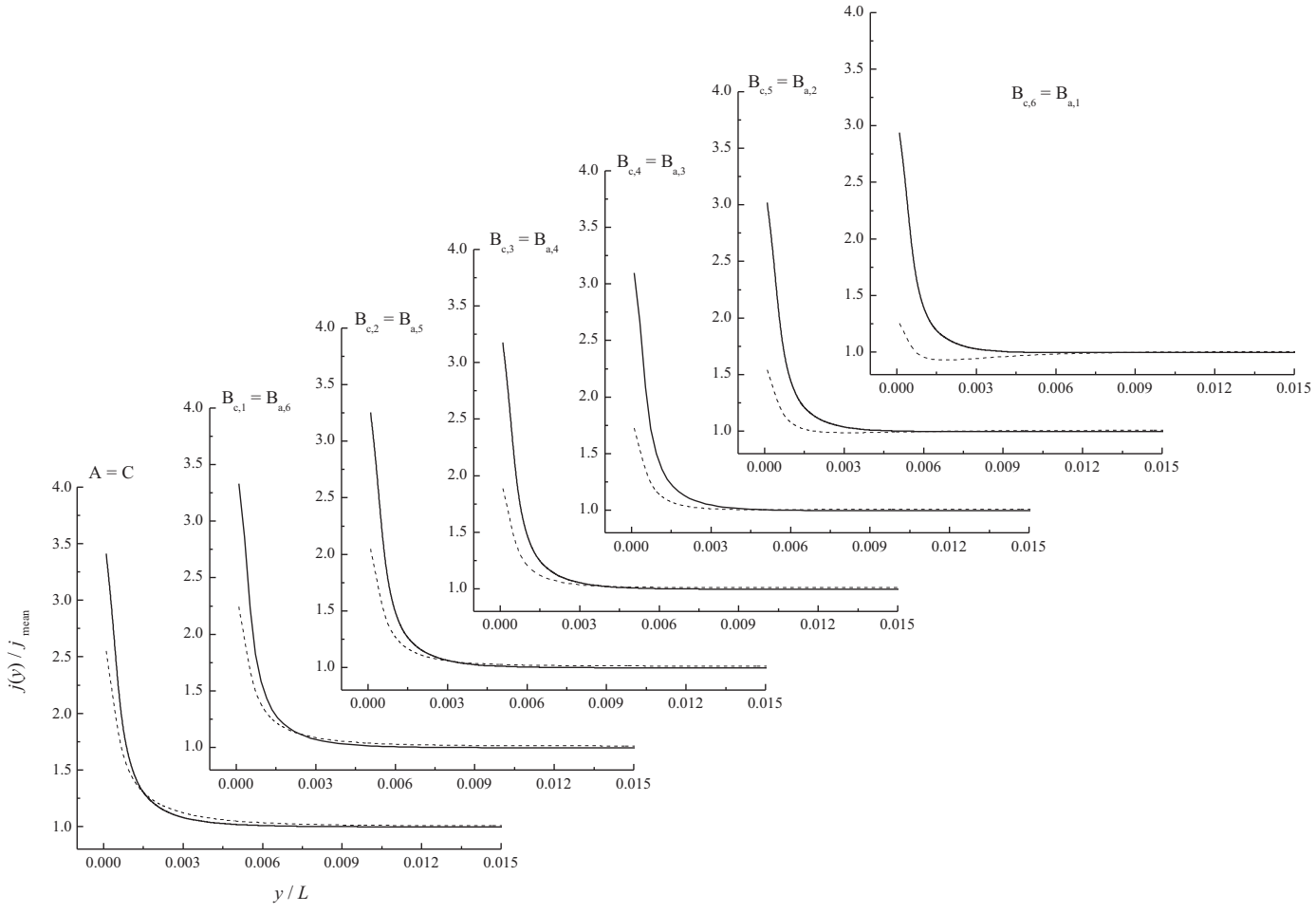

Fig. 5. Comparison of the current density distribution at the electrodes for the two cases represented in Fig. 2. Full line: with entrance and exit regions. Dashed line: without entrance and exit regions.

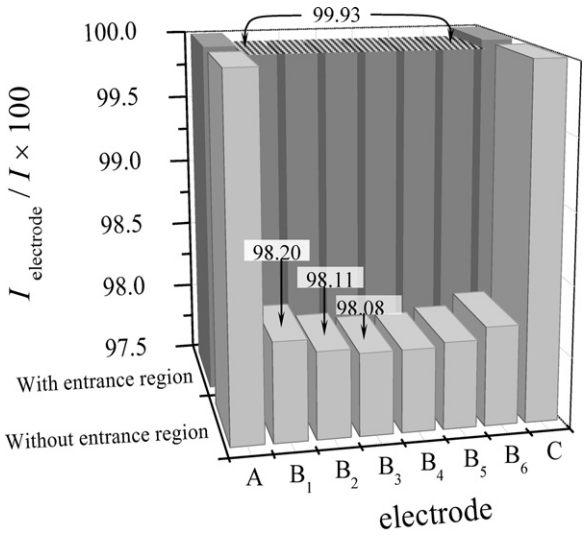

Fig. 6. Comparison of the currents drained at each electrode for the two arrangements represented in Fig. 2.

3.2. Residence time distribution studies

The normalized outlet concentration, termed *E* curve [24], is given by

$$E(t) = \frac{c(t,1)}{\int_0^\infty c(t,1)\mathrm{d}(t/t_{\mathrm{mean}})} \tag{10}$$

$c\,(\mathrm{mol\,m^{-3}})$ being the concentration and $t\,(\mathrm{s})$ the time. In the following experimental data, each curve represents the smoothed values of five independent experiments and a dimensionless time referred to the mean residence time, t_{mean} (s), was used, which was calculated as

$$t_{\mathrm{mean}} = \frac{\int_0^\infty tc(t)\mathrm{d}t}{\int_0^\infty c(t)\mathrm{d}t} \tag{11}$$

The curves in Fig. 7(a) show the change of the normalized outlet concentration at different flow rates of the electrolyte for the reactor with plastic plates in the inlet and exit regions. A main peak and a pronounced tail can be observed, which can be attributed to slow flow zones inside the equipment. To avoid this complication two strategies were used, in the first the plastic plates were removed and the space was completely filled with glass beads, 3 mm diameter. The results are depicted in Fig. 7(b). The second strategy was to fill with glass beads the entrance and exit regions and also the remaining water zone between the water container and the holder for the electrode stack. The response is reported in Fig. 7(c), where the tail is very small and a main narrow peak is detected. Then, a substantial improvement of the hydrodynamic behaviour can be observed, attributable to that the presence of glass beads acts as flow distributors allowing a more uniform flow rate at the different reactors of the bipolar stack. On the other hand, when the plastic plates are removed the reactor works without hydrodynamic entrance length and the developing flow conditions enhance the global mass-transfer coefficient [25], improving the reactor performance.

3.3. In-line production of hypochlorite

The following reactions are expected in this system:

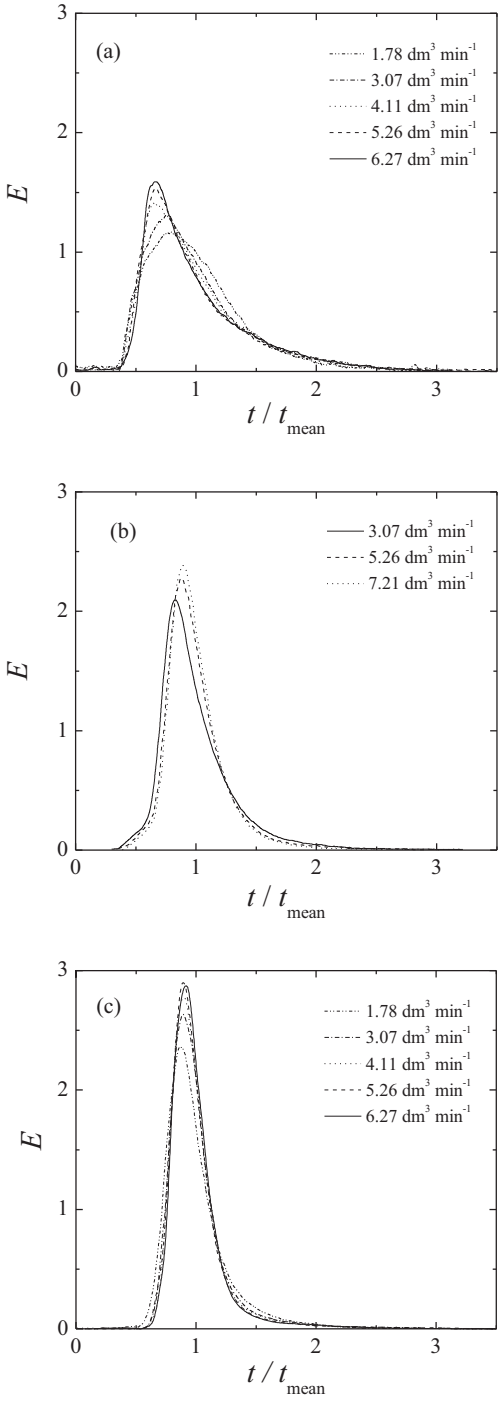

Fig. 7. Experimental residence time distribution. (a) Reactor with plastic plates at the entrance and exit regions. (b) Reactor with glass beads at the entrance and exit regions. (c) Reactor with glass beads at the entrance and exit regions and also in the remaining water zone inside the filter housing.

Hydrogen evolution is the main reaction at the cathode, which is charge-transfer controlled and can be written for basic pH conditions as follows:

$$2H_2O + 2e^- \rightarrow H_2 + 2OH^- \tag{12}$$

and at the anode the competitive reactions take place:

$$2OH^- \rightarrow \tfrac{1}{2}O_2 + H_2O + 2e^- \tag{13}$$

$$2Cl^- \rightarrow Cl_2 + 2e^- \tag{14}$$

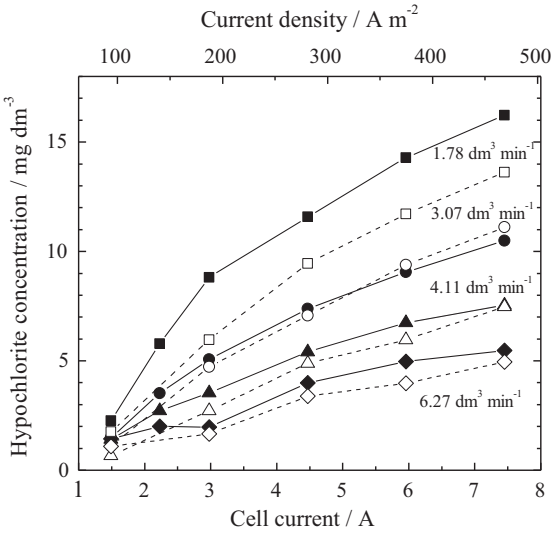

Fig. 8. Hypochlorite concentration as a function of the cell current for different values of volumetric flow rate. Open symbols: reactor with entrance and exit regions. Full symbols: modified reactor with glass beads at the entrance and exit regions and also in the remaining water zone inside the filter housing.

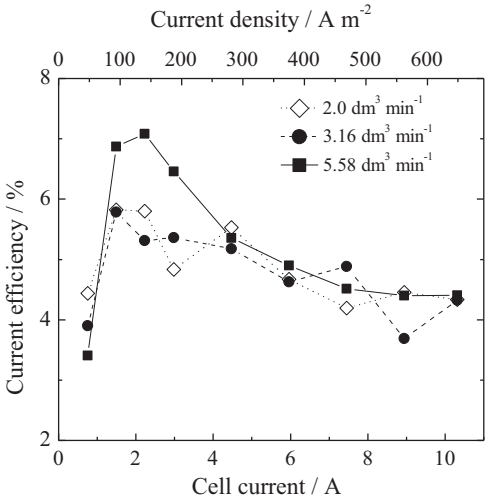

Fig. 9. Current efficiency as a function of the cell current for different values of volumetric flow rate. Reactor with entrance and exit regions.

with a predominant role of reaction (13), with charge-transfer control, for most drinking water conditions.

In the bulk of solution occurs:

$$Cl_2 + 2OH^- \rightarrow ClO^- + Cl^- + H_2O \quad (15)$$

Combining reactions (12)–(15) the overall reaction in the water disinfection reactor results in

$$H_2O + \beta Cl^- \rightarrow H_2 + \tfrac{1}{2}(1-\beta)O_2 + \beta ClO^- \quad (16)$$

being β the current efficiency for reaction (14). Reaction (16) contains the two limiting cases. Thus, for β zero the water splitting reaction is recovered and when β approaches unity the reaction for the electrochemical in-line production of hypochlorite is recuperated. In the above reaction scheme several side reactions, such as: reduction of oxygen, ozone evolution, formation of radicals and reduction of chlorine species were disregarded. The scale formation due to the growth of a cathode precipitate in the presence of calcium and magnesium salts is possible from hard natural water or seawater [26]. This problem is less important for drinking water due to the lower concentration of magnesium and calcium ions. However, the formation of thin films of $Mg(OH)_2$ and $Ca(OH)_2$ inhibits the hypochlorite cathodic reduction [27], increasing the reactor performance.

Experiments for hypochlorite production performed with and without entrance and exit regions for different total currents and volumetric flow rates shown a similar performance of the reactor for both configurations, which is in accordance with the conclusions related to current density distribution, previously reported.

Fig. 8 shows the OCl^- concentration as a function of total current for different values of volumetric flow rate. The open symbols correspond to the reactor with entrance and exit regions and the full symbols to a modified reactor, where the plastic plates were removed and all the empty spaces inside the reactor were filled with glass beads. The concentrations of hypochlorite are in steady-state, which was determined by measuring the conductivity of the solution at the reactor outlet until a constant value was reached. As expected an increase of the cell current enlarges the hypochlorite concentration at the reactor outlet and for a given current the increase of volumetric flow rate diminishes the hypochlorite concentration due to the lower value of the reactor space time. It is also observed that the performance is slightly enhanced for the modified reactor in accordance with the study of residence time distribution, which is more evident for the low value of the volumetric flow rate.

The maximum value of hypochlorite concentration was 25 mg dm^{-3}, achieved for a total current of 10.3 A (648 A m^{-2}) with 2 dm^3 min^{-1} volumetric flow rate, giving a space time yield of 1.39 kg m^3 h^{-1}. In this case the applied voltage was 128 V and 0.44 kWh m^{-3} the specific energy consumption, to give a hypochlorite concentration of 1 ppm. The temperature was 16 °C.

Fig. 9 represents the current efficiency for the hypochlorite production as a function of the total current for different values of volumetric flow rate. Similar values of current efficiency were previously reported [3] for a different electrochemical reactor. According to reaction (16), the low value of current efficiency denotes that the main anodic reaction must be the oxygen evolution. However, the current efficiency shows a maximum, which may be explained by taking into account that because of the low chloride concentration in the solution, reaction (14) depends on the mass-transfer of the chloride to the electrode surface. At low current values, when the current is increased the oxygen evolution enhances the mass-transfer coefficient due to the bubble-induced convection, and thereby increasing the current efficiency for hypochlorite formation. However, at higher currents, very positive anodic potentials, the increase of the partial current of oxygen evolution predominates over that of chlorine formation and low values of current efficiencies are measured. Likewise, the maximum in current efficiency is increased at the higher volumetric flow rate because of the improvement in the mass-transfer conditions.

Thus, the study of current and potential distribution and the use of a procedure to determine the residence time distribution have allowed a rational improvement of the reactor performance. However, for practical applications it becomes necessary to perform long term experiments to establish the best working conditions, taking into account the properties of the drinking water to be treated.

4. Conclusions

- Modelling results for current and potential distribution shows significant effects near the electrode edges, which represent only the 0.5% of the electrode length. Then, the major part of the electrode works under constant current density.
- Edge isolating plastic plates placed at the entrance and exit regions to the electrodes diminish the leakage of current at each

electrode from 2 to 0.1%. In spite of the current distribution is enlarged the major part of the electrode is not affected.

- For the in-line production of hypochlorite, under the examined conditions, the entrance and exit regions are unimportant.
- The hydrodynamic behaviour of the reactor can be improved by removing the plastic plates at the entrance and exit regions and by filling all the empty spaces inside the reactor with glass beads. In this case the reactor performance is slightly enhanced.
- Due to the competition between oxygen and chlorine formation in anodic processes maxima for chlorine (hypochlorite) concentration were found. However, the current efficient is always small.
- The specific energy consumption of this technical reactor with bipolar parallel-plate electrodes is acceptable despite the low value of current efficiency.

Acknowledgements

The authors wish to thank German BMBF/AIF Köln (FKZ 1721X04), BMBF/DLR, MINCYT (Project AL/09/02), ANPCyT and CONICET of Argentina, Universidad Nacional del Litoral, Santa Fe, and Anhalt University, Köthen, for financial and technical support. We also acknowledge Dr. A. Rittel and Dr. T. Iourtchouk (Anhalt University) for practical help.

References

[1] M.E.H. Bergmann, in: C. Comninellis, G. Chen (Eds.), Electrochemistry for the Environment, Springer, New York, 2010, p. 163 (Chapter 7).
[2] M.E.H. Bergmann, T. Iourtchouk, W. Schmidt, G. Nüske, M. Fischer, Perchlorate Formation in Electrochemical Water Disinfection, Nova Science Publishers, New York, 2011.
[3] A. Kraft, Electrochemical water disinfection: a short review, Platinum Metals Review 52 (2008) 177–185.
[4] T. Matsunaga, S. Nakasono, T. Takamuku, J. Grant Burgess, N. Nakamura, K. Sode, Disinfection of drinking water by using a novel electrochemical reactor employing carbon-cloth electrodes, Applied and Environmental Microbiology 58 (1992) 686–689.
[5] M. Okochi, T.-K. Lim, N. Nakamura, T. Matsunaga, Electrochemical disinfection of drinking water using an activated-carbon-fiber reactor capable of monitoring its microbial fouling, Applied Microbiology and Biotechnology 47 (1997) 18–22.
[6] T. Matsunaga, M. Okochi, M. Takahashi, T. Nakayama, H. Wake, N. Nakamura, TiN electrode reactor for disinfection of drinking water, Water Research 34 (2000) 3117–3122.
[7] A.M. Polcaro, A. Vacca, M. Mascia, S. Palmas, R. Pompei, S. Laconi, Characterization of a stirred tank electrochemical cell for water disinfection processes, Electrochimica Acta 52 (2007) 2595–2602.
[8] M.I. Kerwick, S.M. Reddy, A.H.L. Chamberlain, D.M. Holt, Electrochemical disinfection, an environmentally acceptable method of drinking water disinfection? Electrochimica Acta 50 (2005) 5270–5277.
[9] A.M. Polcaro, A. Vacca, M. Mascia, S. Palmas, J. Rodriguez Ruiz, Electrochemical treatment of waters with BDD anodes: kinetics of the reactions involving chlorides, Journal of Applied Electrochemistry 39 (2009) 2083–2092.
[10] A. Vacca, M. Mascia, S. Palmas, A. Da Pozzo, Electrochemical treatment of water containing chlorides under non-ideal flow conditions with BDD anodes, Journal of Applied Electrochemistry 41 (2011) 1087–1097.
[11] I.C.P. Gusmão, P.B. Moraes, E.D. Bidoia, A thin layer electrochemical cell for disinfection of water contaminated with *Staphylococcus aureus*, Brazilian Journal of Microbiology 40 (2009) 649–654.
[12] C.D. Vecitis, M.H. Schnoor, Md.S. Rahaman, J.D. Schiffman, M. Elimelech, Electrochemical multiwalled carbon nanotube filter for viral and bacterial removal and inactivation, Environmental Science and Technology 45 (2011) 3672–3679.
[13] N. Ibl, H. Vogt, in: J.O'M. Bockris, B.E. Conway, E. Yeager, R.E. White (Eds.), Comprehensive Treatise of Electrochemistry, vol. 2, Plenum Press, New York, 1981, pp. 201–208 (Chapter 3).
[14] R. Kodym, M.E.H. Bergmann, K. Bouzek, First results of modelling geometry factors in electrolysis cells for direct drinking water disinfection, in: Proceedings of 56th Annual Meeting of the International Society of Electrochemistry, 26–30 September 2005, Busan, Korea, 2005, p. 896.
[15] R. Kodym, M.E.H. Bergmann, K. Bouzek, Results of modelling electrodes and reactors for the direct electrochemical drinking water electrolysis, in: Proceedings of 57th Annual Meeting of the International Society of Electrochemistry, 27 August–1 September 2006, Edinburgh, UK, 2006, pp. S5–P16.
[16] D. Pletcher, F.C. Walsh, Industrial Electrochemistry, Chapman and Hall, London, 1993, p. 136, (Chapter 2).
[17] M. Kelm, I. Pashalidis, J.I. Kim, Spectroscopic investigation on the formation of hypochlorite by alpha radiolysis in concentrated NaCl solutions, Applied Radiation and Isotopes 51 (1999) 637–642.
[18] A.N. Colli, J.M. Bisang, Evaluation of the hydrodynamic behaviour of turbulence promoters in parallel plate electrochemical reactors by means of the dispersion model, Electrochimica Acta 56 (2011) 7312–7318.
[19] E.R. Henquín, J.M. Bisang, Comparison between primary and secondary current distributions in bipolar electrochemical reactors, Journal of Applied Electrochemistry 39 (2009) 1755–1762.
[20] G.A. Prentice, C.W. Tobias, Finite difference calculation of current distributions at polarized electrodes, AIChE Journal 28 (1982) 486–492.
[21] E.R. Henquín, J.M. Bisang, Effect of leakage current on the primary current distribution in bipolar electrochemical reactors, Journal of Applied Electrochemistry 37 (2007) 877–886.
[22] K. Bouzek, K. Børve, O.A. Lorentsen, K. Osmundsen, I. Rousar, J. Thonstad, Current distribution at the electrodes in zinc electrowinning cells, Journal of the Electrochemical Society 142 (1995) 64–69.
[23] D. Bergner, K. Hannesen, in: K. Wall (Ed.), Modern Chlor-Alkali Technology, vol. 3, Ellis Horwood Ltd., Chichester, 1986, pp. 162–177 (Chapter 13).
[24] P.V. Danckwerts, Continuous flow systems. Distribution of residence times, Chemical Engineering Science 2 (1953) 1–13.
[25] A.N. Colli, J.M. Bisang, Validation of theory with experiments for local mass transfer at parallel plate electrodes under laminar flow conditions, Journal of the Electrochemical Society 160 (2013) E5–E11.
[26] G.H. Kelsall, Hypochlorite electrogeneration. I. A parametric study of a parallel plate electrode cell, Journal of Applied Electrochemistry 14 (1984) 177–186.
[27] A.T. Kuhn, H. Hamzah, G.C.S. Collins, The inhibition of the cathodic reduction of hypochlorite by films deposited at the cathode surface, Journal of Chemical Technology and Biotechnology 30 (1980) 423–428.